Enhanced second-harmonic generation from individual metallic nanoapertures

Peter Schön,[1] Nicolas Bonod,[1] Eloïse Devaux,[2] Jérôme Wenger,[1] Hervé Rigneault,[1] Thomas W. Ebbesen,[2] and Sophie Brasselet[1,*]

[1]*Institut Fresnel, Aix-Marseille Université, CNRS, Ecole Centrale Marseille, Domaine Universitaire St Jérôme, 13013 Marseille, France*

[2]*Institut de Science et Ingénierie Supramoléculaires, Université de Strasbourg, CNRS, 8 allée G. Monge, 67000 Strasbourg, France*

**Corresponding author: sophie.brasselet@fresnel.fr*

Received September 15, 2010; accepted October 27, 2010; posted November 9, 2010 (Doc. ID 135004); published November 30, 2010

We demonstrate the ability of single-subwavelength-size nanoapertures fabricated in a gold metal thin film to enhance second-harmonic generation (SHG) as compared to a bare metal film. Nonlinear microscopy imaging with polarization resolution is used to quantify the SHG enhancement in circular and triangular nanoaperture shapes. The dependence of the measured SHG enhancement on circular aperture diameters is seen to originate from both phase retardation effects and field enhancements at the nanoaperture edge. Triangular nanoapertures exhibit superior SHG enhancement compared with circular ones, as expected from their noncentrosymmetric shape.

OCIS codes: 050.6624, 190.4350, 180.4315.

The understanding and optimization of nonlinear optical properties of metallic nanostructures is a major issue for future applications in nanophotonics [1]. Nonlinear quadratic effects in metals have been known for decades to be significant at the metal–outer-medium two-dimensional interface where centrosymmetry is broken [2]. This effect can lead to very large second-harmonic generation (SHG) responses, enhanced by plasmon resonances, as recently observed in single-metal nanoparticles [3].

Among the promising metallic structures for nanoplasmonics, metal nanoapertures have shown their ability to significantly enhance optical fields in the nanovolume that they define [4]. Previous works have addressed SHG responses in metallic apertures of micrometric size [5], subwavelength apertures with periodic surface corrugations [6], or nanoaperture arrays [7–9]. However, the influence of the size and shape of a single nanoaperture to enhance the SHG signal still remains an open question. In this work, we explore the ability of isolated metallic nanoapertures of subwavelength dimensions to enhance SHG signals in circular and triangular shape structures.

The nonlinear microscope developed in this work uses a tunable Ti:sapphire laser (150 fs, 80 MHz, wavelength 850 nm) beam reflected by a dichroic mirror and focused on the sample by a high-NA objective (×60, 1.2 NA), leading to an optical resolution of 300 nm in the sample plane. The backward emitted signal is collected by the same objective and directed to a polarization beam splitter that separates the beam toward two avalanche photodiodes. Images are performed by scanning the sample on a piezoelectric stage. For polarization-resolved measurements, the linear polarization of the incident laser beam is continuously rotated in the sample plane by an achromatic half-wave plate mounted on a step rotation motor at the entrance of the microscope [10]. The nanoapertures, whose sizes range from 125 nm to 425 nm, are formed by a focused ion beam in a 200-nm-thick gold film fixed to a glass coverslip using a 10-nm-thick chromium adhesion layer and studied in air.

The dominant SHG contribution from the nanostructure can be modeled by a nonlinear tensor exhibiting a major diagonal coefficient $\chi^{(2)}_{nnn}$ (n being the normal direction to the metal-air surface) and weaker off-diagonal ($\chi^{(2)}_{ntt}, \chi^{(2)}_{tnt}, \chi^{(2)}_{ttn}$) contributions (typically by a factor of 10) [11]. In the case of nanoapertures lying in the microscope sample plane (X, Y) [Fig. 1(a)], the nonlinear dipole (i component) $p_i^{2\omega} = \sum_{j,k} \chi^{(2)}_{ijk} E^{\omega}_j E^{\omega}_k$ appears in two types of regions: the aperture edge surface ($p^{2\omega}_{a,i}$ lying in the (X, Y) plane) and the metal film surface region illuminated within the excitation volume around the aperture ($p^{2\omega}_{s,i}$ along Z). This latter contribution originates from the nonlinear coupling involving the Z components of the excitation fields E^{ω} in the focused beam. It is expected to be lower than the aperture edge contribution by an order of magnitude, as expected from the field maps calculated at high NA [12].

Figure 1(b) shows a typical scanning SHG image of a nanoaperture, which resembles a diffraction-limited spot due to the subwavelength size of the object. A weak nonvanishing signal is observed from the background, owing to a remaining contribution from the bare metal surface. The spectrum observed from this background radiation contains a dominant SHG signal and a spectrally shifted two-photon luminescence signal [Fig. 1(c)], originating from interband excitations in the gold metal. The SHG experiments are performed using an optical filter selecting the spectral region around the harmonic signal. To compare the SHG efficiency from different structures' shapes and sizes, the measured SHG signal is summed over 90 incident linear polarization directions varying between 0° and 360° relative to X. The enhancement factor, defined by the ratio between this averaged SHG signal and the averaged bare metal surface SHG response, is represented in Fig. 2(a) for circular apertures as a function of their diameter. This procedure allows, in particular, averaging out possible nanoaperture shape irregularities. A signal enhancement of about 2 for diameters around

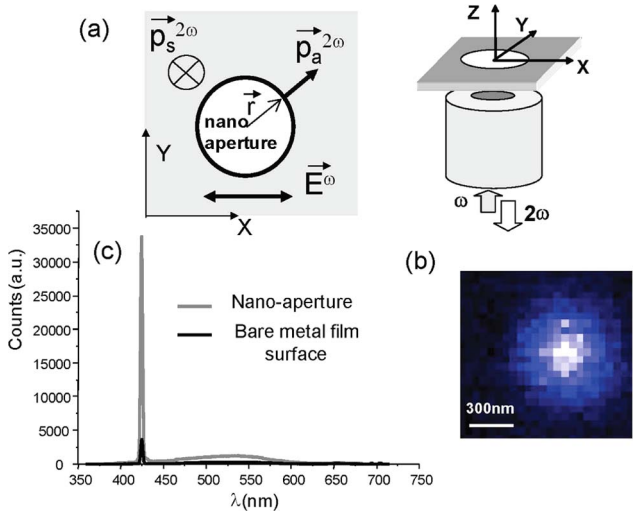

Fig. 1. (Color online) (a) Nonlinear induced dipoles in a metal nanoaperture. (b) Experimental scheme of the nonlinear microscopy imaging and SHG image of a circular nanoaperture (diameter 195 nm). (c) Emission spectrum from a nanoaperture and the bare metal surface, measured using a spectrograph at the exit of the microscope (diameter 195 nm, excitation: horizontal polarization). Typical average power at the objective focus: a few milliwatts.

220 nm can be observed, even though the structure is centrosymmetric. Interestingly, nanostructuring plasmonic structures by removing matter therefore leads to an improvement of their SHG response.

In circular centrosymmetric structures of hundreds of nanometer size, similar to spherical metal nanoparticles, the SHG signal is expected to arise primarily owing to phase-retardation effects between nonlinear emitters around the interface [13]. To model the observed behavior, the radiation from a collection of nonlinear dipoles $p_n^{2\omega}(\vec{r}_n)$ located at positions $\vec{r}_n$ along the interface was calculated accounting for the $E_j^{\omega}(\vec{r}_n)$ excitation-field local polarization [12]. Although this assumption does not account for the scattered contribution from the apertures, it allows exhibiting the geometrical features of their SHG response. For this calculation, nonlinear induced dipoles were placed regularly on the aperture edge and film surfaces using a mesh size of 10 nm. The SHG signal is obtained by summing coherently the radiated fields from these nonlinear dipoles after the passage of the high-NA collection objective [14]. This model shows that thanks to phase-retardation effects, the SHG response from circular nanoapertures growths with their size [Fig. 2(a), dotted line]. However, it does not explain the origin of the observed maximum.

Modeling the overall SHG process requires also accounting for the scattered contribution from the structure itself. The calculation of the field inside circular nanoapertures was carried out by a rigorous differential method able to solve Maxwell equations in single subwavelength sized apertures [15]. In this formalism, the field is developed onto a Fourier–Bessel basis. A first integration under a planar wave illumination [Fig. 2(b)] leads to the calculation of the electromagnetic field in the substrate and superstrate, and a second integration to the knowledge of the three spatial components of the field inside the aperture. These calculated fields are introduced at two levels. First, their normal components at the ω frequency $E_n^{\omega}(\vec{r}_n)$, calculated at 1 nm distance from the interface [Fig. 2(c)], are directly introduced in the expression of the nonlinear induced dipoles on the whole aperture edge surface. Second, the local enhancement at the 2ω frequency is introduced as a scaling factor for the nonlinear radiated field. Note that the nanoapertures' behavior at these two frequencies is very different: whereas they behave like a lossy dielectriclike waveguide at the 425 nm SHG wavelength, they are metal-like at 850 nm with a cutoff diameter of about 280 nm. This model is still a simplification in the sense that (i) it is based on planar waves excitation, (ii) the 2ω enhancement response from the structure is treated in a linear diffraction regime, not accounting for higher order coupling between 2ω and ω fields. Nevertheless, it shows already a good agreement with the observed SHG size maximum [Fig. 2(a), dashed line]. This result shows that the nanoaperture interface acts advantageously for both the generation of nonlinear SHG radiated fields and their enhancement.

Whereas SHG enhancement is quite modest in circular apertures due to their centrosymmetric shape, higher enhancement factors could be observed in triangular apertures whose shapes are intrinsically noncentrosymmetric [Fig. 3(a)]. The size dependence of the SHG response is in this case, however, more complex to interpret because of the visible shape deformations in the structures. The influence of this shape on the SHG responses was further ascertained by polarization dependence studies, which is a powerful way to probe structural information in subwavelength size objects [10]. Typical examples of measured SHG polarization responses are depicted in Fig. 3(b). Pure

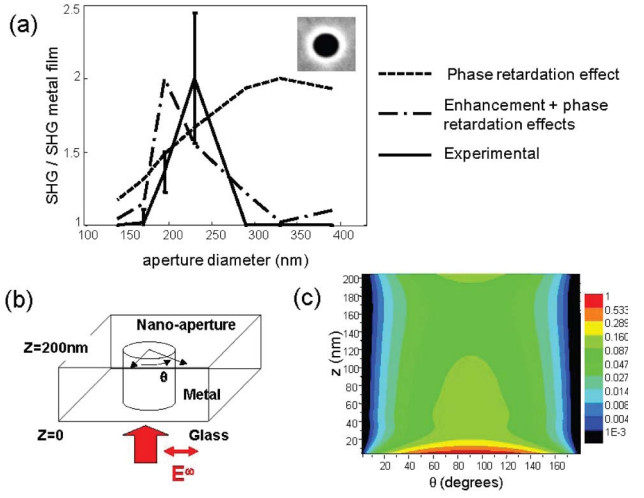

Fig. 2. (Color online) (a) SHG enhancement factor (averaged over all incident polarizations) relative to the signal from the bare metal surface for circular apertures, as a function of their diameter. Continuous line, experimental data. Dashed line, simple dipole model. Semidashed line, model including the calculated field enhancement factors. Theoretical curves are normalized to the experimental maximum. The inset is a typical electron microscopy image of the studied structures. (b) Geometry used for the calculation of the scattered electric field. (c) Calculated normalized map of the radial component $|E_n^{\omega}|$ of the field as a function of the angle around the surface (θ) and the height (Z) relative to the glass substrate, in a 195 nm diameter aperture. The incident field is polarized along the X direction ($\theta = 90°$).

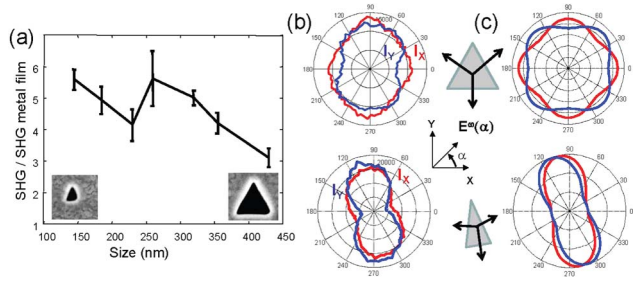

Fig. 3. (Color online) (a) Measured SHG enhancement factor for triangular apertures as a function of their side length. The insets are typical electron microscopy images of the studied structures. (b) Polar representation of the experimental polarization-resolved SHG response analyzed along the X (red) and Y (blue) analysis directions for two triangular nanoapertures of 320 nm size (top) and 170 nm diameter (bottom). (c) Phenomenological normalized SHG polarization responses calculated from three centered nonlinear dipoles (black arrows), whose orientations are calculated from the normal directions to the drawn triangles faces. Above, triangle of edges of equal sizes. Below, lower basis of the triangle reduced by a factor of 2, and tilt angle by −10° relative to its original orientation. A polarization-independent background of 30% of the maximum intensity is added.

triangular apertures of large sizes (>200 nm) show typical four lobe patterns expected from their third-order symmetry [16]. Modeled SHG polarization responses from a pure third-order symmetry structure made of three nonlinear dipoles centered on the optical axis and illuminated by a planar wave, including a polarization-independent background that may occur from the bare-metal-surface contribution, show similarities [Fig. 3(c)]. In smaller structures, deviations toward dipolarlike responses can be observed, as expected from the deformed triangles in electron microscopy images. Nevertheless, a SHG enhancement greater than 4 can be readily observed with triangular apertures of sizes below 350 nm. We have demonstrated that metal nanoapertures of size much below the wavelength can enhance SHG responses comparing to a planar metal surface. The relative dependence of the enhancement factors to the structure size can be understood in circular apertures from a phenomenological model accounting for phase-retardation effects at the nanoaperture interface and local fields enhancement factors. Noncentrosymmetric shapes are seen to be promising to further enhance SHG responses. We believe that the methodology developed here is able to guide nonlinear responses optimization in metal nanoapertures and related structures.

This work is supported by the French Agence Nationale de la Recherche under the program ANR JC 2007 and the project NLO-Shaping JC07-195504 and is partially supported by the ERC grant 227577 (“Plasmonics”).

References

1. A. Bouhelier, M. Beversluis, A. Hartschuh, and L. Novotny, Phys. Rev. Lett. **90**, 013903 (2003).
2. P. Guyot-Sionnest, W. Chen, and Y. R. Shen, Phys. Rev. B **33**, 8254 (1986).
3. J. Butet, J. Duboisset, G. Bachelier, I. Russier-Antoine, E. Benichou, C. Jonin, and P.-F. Brevet, Nano Lett. **10**, 1717 (2010).
4. C. Genet and T. W. Ebbesen, Nature **445**, 39 (2007).
5. T.-D. Onuta, M. Waegele, C. C. DuFort, W. L. Schaich, and B. Dragnea, Nano Lett. **7**, 557 (2007).
6. A. Nahata, R. A. Linke, T. Ishi, and K. Ohashi, Opt. Lett. **28**, 423 (2003).
7. M. Airola, Y. Liu, and S. Blair, J. Opt. A **7**, S118 (2005).
8. J. A. H. van Nieuwstadt, M. Sandtke, R. H. Harmsen, F. B. Segerink, J. C. Prangsma, S. Enoch, and L. Kuipers, Phys. Rev. Lett. **97**, 146102 (2006).
9. T. Xu, X. Jiao, G. P. Zhang, and S. Blair, Opt. Express **15**, 13894 (2007).
10. S. Brasselet, V. Le Floc’h, F. Treussart, J. F. Roch, J. Zyss, E. Botzung-Appert, and A. Ibanez, Phys. Rev. Lett. **92**, 207401 (2004).
11. C. W. Teplin and C. T. Rogers, J. Appl. Phys. **96**, 3626 (2004).
12. B. Richards and E. Wolf, Proc. R. Soc. Lond., Ser. A **253**, 358 (1959).
13. J. I. Dadap, J. Shan, and T. Heinz, J. Opt. Soc. Am. B **21**, 1328 (2004).
14. N. Sandeau, L. Le Xuan, D. Chauvat, C. Zhou, J.-F. Roch, and S. Brasselet, Opt. Express **15**, 16051 (2007).
15. E. Popov, M. Nevière, A. Sentenac, N. Bonod, A.-L. Fehrembach, J. Wenger, P.-F. Lenne, and H. Rigneault, J. Opt. Soc. Am. A **24**, 339 (2007).
16. S. Brasselet and J. Zyss, J. Opt. Soc. Am. B **15**, 257 (1998).